Impact of Confining Stress on Capillary Pressure Behavior During Drainage Through Rough Fractures

Geophysical Research Letters

RESEARCH LETTER
10.1029/2019GL082744

Key Points:
- In-plane interface curvature impacts signature of capillary pressure during drainage in rough fractures
- Hierarchical avalanche size distribution is consistent with a system that exhibits self-organized criticality
- Power spectrum of capillary pressure suggests increased self-organization as confining stress increases

Supporting Information:
- Supporting Information S1

Correspondence to:
R. Juanes,
juanes@mit.edu

Citation:
da Silva, J. A., Kang, P. K., Yang, Z., Cueto-Felgueroso, L., & Juanes, R. (2019). Impact of confining stress on capillary pressure behavior during drainage through rough fractures. *Geophysical Research Letters*, *46*, 7424–7436. https://doi.org/10.1029/2019GL082744

Received 7 MAR 2019
Accepted 21 JUN 2019
Accepted article online 3 JUL 2019
Published online 15 JUL 2019

Impact of Confining Stress on Capillary Pressure Behavior During Drainage Through Rough Fractures

Josimar A. da Silva[1], Peter K. Kang[2], Zhibing Yang[3], Luis Cueto-Felgueroso[4,5], and Ruben Juanes[1,5]

[1]Department of Earth, Atmospheric, and Planetary Sciences, Massachusetts Institute of Technology, Cambridge, MA, USA, [2]Department of Earth Sciences, University of Minnesota, Twin Cities, Minneapolis, MN, USA, [3]State Key Laboratory of Water Resources and Hydropower Engineering Science, Wuhan University, Wuhan, China, [4]School of Civil and Environmental Engineering, Technical University of Madrid, Madrid, Spain, [5]Department of Civil and Environmental Engineering, Massachusetts Institute of Technology, Cambridge, MA, USA

Abstract We study, numerically, the behavior of capillary pressure (P_c) during slow immiscible displacement in a rough fracture as a function of the degree of fracture aperture heterogeneity that results from two distinct mechanisms: normal confining stress and fracture surface correlation. We generate synthetic self-affine rough fractures at different correlation scales, solve the elastic contact problem to model the effect of confining stress, and simulate slow immiscible displacement of a wetting fluid by a nonwetting one using a modified invasion percolation model that accounts for in-plane curvature of the fluid-fluid interface. Our modeling results indicate that the power spectral density, $S(f)$, of P_c, can be used to qualitatively characterize fracture aperture heterogeneity. We show that the distribution of forward avalanche sizes follows a power law $N_f(S_f) \propto S_f^{-\alpha}$, with exponent $\alpha = 2$, in agreement with previously reported values for porous media and equal to the expected theoretical exponent for a self-organized criticality process.

1. Introduction

The slow immiscible displacement of a wetting fluid by a nonwetting one in porous media, a process known as drainage, is governed by capillary forces (Holtzman et al., 2012; Lenormand et al., 1983, 1988; Måløy et al., 1992; Wilkinson & Willemsen, 1983). This flow regime has a number of important practical applications, such as geological CO_2 storage (Pruess, 2008), underground nuclear waste disposal (Nuske et al., 2010), and secondary oil migration (Meakin et al., 1992). During slow drainage in porous media, the invasion process is marked by intermittency with bursts of fluid invasion, or avalanches, in which capillary pressure fluctuates rapidly, followed by quiescent periods with no interface motion (Berg et al., 2013; Biswas et al., 2018; Furuberg et al., 1996; Haines, 1930; Måløy et al., 1992; Moebius & Or, 2014). Experiments and numerical simulations have shown that these rapid capillary pressure fluctuations depend on the degree of organization of the porous medium (Biswas et al., 2018; Moura et al., 2017).

While porous rocks account for the bulk of fluid volume in the subsurface, in low permeability media most of the fluid flow may take place through networks of interconnected fractures. Natural fractures differ significantly from porous media because they consist of rough surfaces with variable degree of roughness and a distinct self-affine correlation structure (Brown, 1995; Brown & Scholz, 1985a; Power & Tullis, 1991). Another key difference is that, in its natural setting, a single fracture is subject to large geological confining stresses that compress the two sides of the rough fracture and reduce the available space for fluid flow (Brown & Scholz, 1985b; Jaeger & Cook, 1979; Kang et al., 2016; Pyrak-Nolte & Nolte, 2016; Pyrak-Nolte & Morris, 2000; Wang & Cardenas, 2016; Zimmerman & Bodvarsson, 1996). Thus, given these differences relative to porous media, it is unclear whether capillary pressure during slow drainage through a rough fracture, at different confining stresses, behaves similarly to its porous media counterpart.

Previous investigations of drainage through rough fractures have focused on the impact of confining stress on macroscopic properties such as relative permeability and pressure-saturation relations. Experiments and numerical modeling have shown that increasing confining stress increases fracture roughness and fracture

contact area, resulting in lower relative permeability values and a reduction in displacement efficiency (Bertels et al., 2001; Huo & Benson, 2016; Lian & Cheng, 2012; McDonald et al., 1991; Pyrak-Nolte et al., 1990; Watanabe et al., 2015). Similarly, the capillary pressure-saturation relation for slow drainage through rough fractures has been modeled using empirical and semianalytic models obtained for porous media, such as Brooks-Corey (Brooks & Corey, 1964), van Genuchten (van Genuchten, 1980), and ν-type models (Watanabe et al., 2015). Measurements of the capillary pressure-saturation relationship during slow drainage through a natural rough fracture have shown good agreement with the Brooks-Corey function (Reitsma & Kueper, 1994), whereas numerical simulations using a continuum-based model indicates that both Brooks-Corey and van Genuchten models yield similar results (Yang et al., 2013). These experiments and numerical simulations were conducted under prescribed pressure, which is slowly increased in order to force invasion into the fracture. Here, in contrast, we are interested in the capillary pressure behavior for a flow rate controlled boundary condition, which allows capillary pressure to vary as the invasion into the fracture proceeds.

Measurements and simulations of capillary pressure (P_c) during slow drainage have been extensively reported for the case of imposed flow rate in porous media (Aker et al., 2000; Biswas et al., 2018; Furuberg et al., 1996; Måløy et al., 1992; Moebius & Or, 2014; Moura et al., 2015, 2017). Similar measurements for a rough fracture are scarce. Persoff and Pruess (1995) were the first ones to report, experimentally, P_c variations during slow drainage through a rough fracture. In their experimental configuration, the fracture aperture structure was kept constant and the boundary conditions were changed. They observed strong phase interference and cyclical pressure variations, associated with flow instabilities, that were interpreted as the interaction between capillary pressure and pressure drop due to viscous flow. Auradou et al. (2003) numerically modeled P_c in a vertical gouge-filled fracture but did not investigate the sensitivity of P_c to the degree of fracture aperture heterogeneity. Other studies of drainage through rough fractures have focused, for example, in the quantification of amount of trapping of the defending phase (Yang et al., 2016) and crossover from capillary fingering to viscous fingering (Chen et al., 2017; Chen, Guo, Wu, et al., 2018; Chen, Wu, Fang, et al., 2018).

In addition to characterizing P_c variations, we are interested in characterizing avalanches, or invasion bursts, associated with the rapid capillary pressure fluctuations in rough fractures. The scaling behavior of avalanche size is well known for drainage in porous media (Aker et al., 2000; Biswas et al., 2018; Maslov, 1995), but it is unclear whether such scaling extends to slow drainage through a rough fracture.

In our numerical simulations, we first generate self-affine fracture surfaces with different degrees of spatial correlation (Brown, 1995), solve the elastic contact problem between both surfaces to model the impact of confining stress (Kang et al., 2016), and then perform simulations of slow drainage using both the original invasion percolation algorithm (Wilkinson & Willemsen, 1983) and a modified invasion percolation method that accounts for the fluid-fluid in-plane curvature (Glass et al., 1998, 2003 ; Yang et al., 2012). Here, we design our numerical experiment to mimic a condition of controlled volume (constant flow rate). The idea behind "volume control" is that the displacement—assumed to be quasi-static—is conducted one pixel at a time, which permits in turn to track the minimum capillary entry pressure (or, simply, the capillary pressure) at each single-pixel invasion event. This capillary pressure record exhibits positive and negative jumps through the displacement process. This differs from "pressure control," a protocol in which, even if the displacement is assumed to be quasi-static, the capillary pressure is monotonically increasing, with associated avalanches in the volume of fluid displaced. We then analyze the behavior of the capillary pressure as a function of the degree of heterogeneity in the aperture field that results from different confining stresses and different fracture aperture correlation lengths.

2. Rough Fracture Generation and Flow Modeling

2.1. Fracture Aperture Generation

We construct synthetic rough-walled fractures using the spectral synthesis method (Brown, 1995; Kang et al., 2016). In this method, each fracture surface is decomposed into its power spectral density function and a phase spectrum. The power spectral density $G(k)$ exhibits a power law decay with wavenumber $k = 2\pi/\lambda$, where λ is wavelength, as

$$G(k) = Ck^{-\xi}, \tag{1}$$

where the exponent ξ is related to the fractal dimension D of the fracture surface as $D = (7 - \xi)/2$ and the intercept C is determined by the standard deviation of surface heights σ_f . Measurements of surface

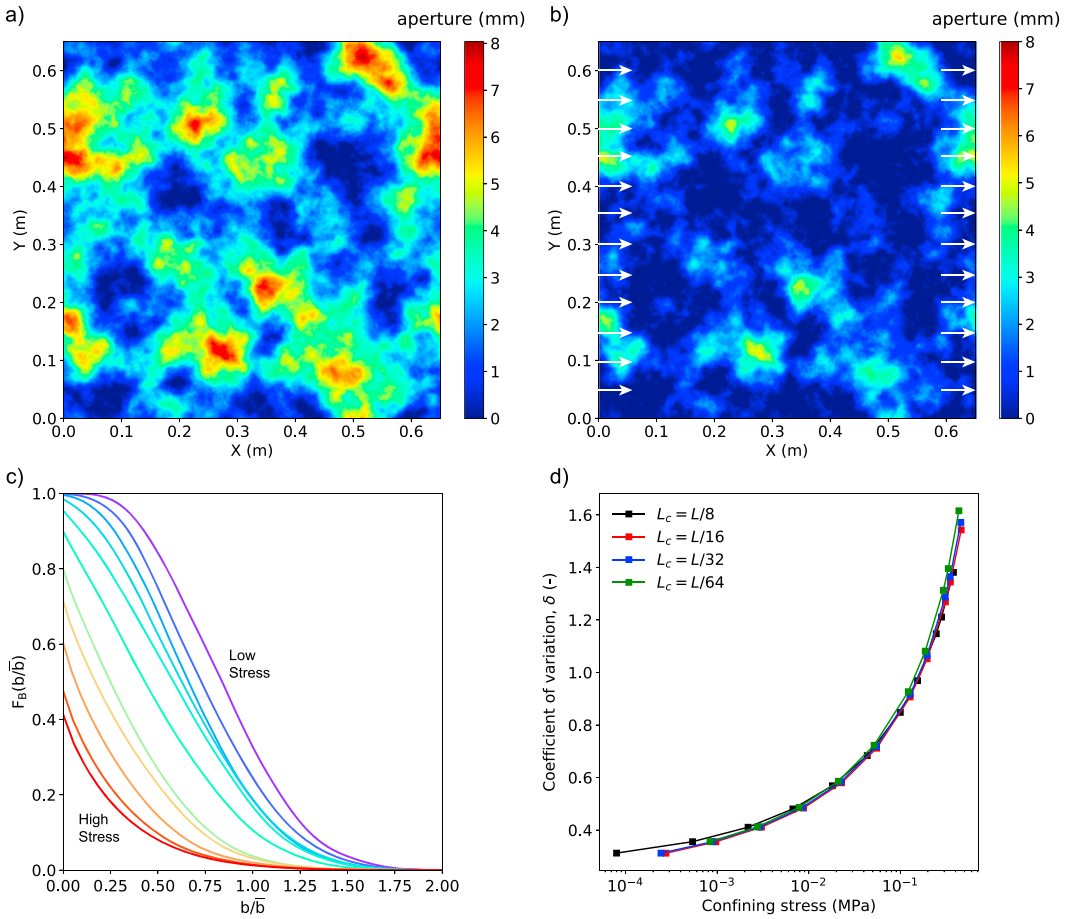

Figure 1. (a) Example of fracture aperture at low confining stress, $\sigma_n = 0.02$ MPa. Here, we show an aperture field generated from self-affine fracture surfaces with mismatch length scale $L_c = L/8$. (b) Same as (a) but for a larger confining stress, $\sigma_n = 0.15$ MPa. The white arrows indicate the flow direction. (c) Cumulative aperture distribution, $F_B(b/\bar{b})$, at different confining stresses. Each line corresponds to the average of 20 fracture aperture fields. (d) Average coefficient of variation, $\delta = \sigma_b/\bar{b}$, where σ_b is the aperture standard deviation and $\bar{b}$ is the mean fracture aperture, as a function of confining stress.

roughness in several rock fractures have shown that D tends to fall in the range $2 \leq D \leq 2.5$ (Brown & Scholz, 1985a). Values of D close to 2 and 2.5 result in smoother and rougher surfaces, respectively (Brown & Scholz, 1985a; Power & Tullis, 1991). Here we fix $D = 2.5$ to construct rough surfaces.

The phase spectrum of an individual fracture surface is assumed to be a random process independent of the frequency. Thus, different fracture surfaces can be generated by changing the seed used in the random number generator. Measurements of the fracture surface heights have shown that they are uncorrelated at small wavelengths and correlated at long wavelengths (Brown & Scholz, 1985a). To model this process, Kang et al. (2016) introduced a phase correlation function $\gamma = \frac{1}{2}[1 + \text{erf}(-\frac{k-k_c}{\mu})]$, where μ is a model parameter that determines the rate of correlation decay, here fixed at $\mu = 6$. $k_c = 1/L_c$ is the wavenumber at which the phase correlation between top and bottom surfaces is 0.5, and L_c is the mismatch length scale, beyond which the fracture surfaces are correlated. Here we choose $L_c = L/8, L/16, L/32, L/64$, where L is the domain size, to investigate also the impact of the fracture correlation length, along with confining stresses, on the capillary pressure behavior.

Based on previous work, we construct a numerical model of a synthetic fracture with dimensions of 0.65 m × 0.65 m (Neuweiler et al., 2004; Yang et al., 2012). We discretize the fracture surface using $1,024 \times 1,024$ pixels, where each pixel has dimensions $dx = dy = 0.63$ mm, and generate several fracture surfaces using different seeds for the random number generator. Figure 1a shows an example of the resulting fracture aperture field.

2.2. Modeling the Impact of Confining Stress on Fracture Aperture

We consider fracture apertures generated from self-affine fracture surfaces with different correlation lengths. To model the impact of confining stress on the fracture aperture, we assume a linear elastic medium and follow the procedure described in Kang et al. (2016). The fracture aperture is represented by its composite topography (Brown, 1995), which is given by the sum of the fracture surface heights relative to a parallel reference plate.

We model the deformation of the aperture field, represented by its composite topography, as a flat rigid surface makes contact with it. The deformation of the composite topography is constrained such that there is no interpenetration between the two surfaces. In the areas where interpenetration occurs, resulting in an aperture less than or equal to zero, the compressive normal stress $S(x, y)$ is positive and the composite topography surface deforms elastically. In areas where the aperture is greater than zero, the compressive stress is zero. This is a mixed boundary value problem, where displacements are defined over parts of the surface and normal stress over the remainder of the surface.

To model the elastic displacement of the composite topography due to an applied normal stress $S(x, y)$, we use the analytical solution for normal displacement due to a point force on an elastic half-space known as Boussinesq solution, $B(r) = \frac{(1-\nu)}{2\pi G}\frac{1}{r}$, where r is the distance to where the point load is applied, $r = \sqrt{(x-x')^2 + (y-y')^2}$, ν is the Poisson ratio, and G is the shear modulus. The normal displacement $w(x, y)$ due to stress field $S(x, y)$ is obtained by convolution of the Boussinesq solution: $w(x, y) = \iint S(x', y')B(r)\mathrm{d}x'\mathrm{d}y'$ (Andrews, 1988; Unger & Mase, 1993) . The solution to the mixed boundary value problem is obtained using the two-dimensional Fast Fourier Transform (FFT), which makes the solution biperiodic (Kang et al., 2016). In our simulations, we used $G = 20$ GPa and $\nu = 0.25$, which are values corresponding to Berea sandstone under confining stress around 30 MPa (Mavko et al., 2009).

The elastic deformation is controlled by the effective stress, which is the difference between confining total stress and fluid pressure. Because we assume quasi-static displacements, the viscous pressure drop is zero, and the only contribution to pressure differences within the fracture is the capillary pressure. Values of capillary pressure in our system are ~1 kPa, several orders of magnitude smaller than confining stresses ~1 MPa (Figure 1d). Thus, it is reasonable to assume that the influence of fluid pressure variations within the fracture can be neglected.

The solution is obtained by iteratively updating $S(x, y)$ until the stress field satisfies the zero-interpenetration condition everywhere. During the iteration, where there is an overlap (negative fracture aperture), the normal stress is changed to be more compressive. The normal stress is used to recalculate the elastic displacement, the aperture is then recalculated, and the procedure is repeated until a threshold value is met. Solving the elastic deformation problem does lead to different fracture geometry compared with simply removing the overlaps between the two surfaces, especially at high normal stress.

As expected, a high confining stress leads to large contact area between the fracture surfaces, while a low confining stress results in almost no contact area. This behavior can be synthesized by computing variations in the cumulative fracture aperture, $F_B(b)$, with the confining stress (Figure 1c). Increasing the confining stress causes the mean fracture aperture to decrease and the standard deviation to increase. We have verified that the shape of F_B is nearly independent of the fracture correlation length scale, indicating that variations in the confining stress exert the main control in the cumulative fracture aperture distribution.

2.3. Modified Invasion Percolation (MIP)

Invasion Percolation (IP) was introduced by Wilkinson and Willemsen (1983) as an extension of ordinary percolation (Broadbent & Hammersley, 1957) to model the slow immiscible displacement of a wetting fluid by a nonwetting one in porous media. In the IP model, it is assumed that flow is quasi-static, and therefore, viscous forces vanish and flow is controlled by the capillary pressure at the interface between the two fluids.

To simulate slow drainage through horizontal rough fractures shown in Figure 1, we use the original IP model (Wilkinson & Willemsen, 1983) and a MIP model to account for the fluid-fluid interface curvature on the plane of the fracture (Glass et al., 1998, 2003; Yang et al., 2012). In both IP models, we allow for trapping of the defending fluid. The MIP model was originally proposed by Glass et al. (1998)—they introduced a "curvature number" C controlling the influence of the in-plane curvature relative to the aperture-induced curvature. Later, this approach to account for the in-plane curvature was modified by Yang et al. (2012), who proposed local fitting of a circle to estimate the in-plane curvature along the fluid-fluid interface. These

studies have shown that in-plane curvature can significantly influence the predictions of fluid trapping (Glass et al., 2003; Yang et al., 2016).

We conceptualize the fracture aperture as a square lattice where each pixel has a fourfold connectivity to the neighbor pixels on the lattice. Flow occurs from the left boundary to the right boundary of the fracture, with no flow through the top and bottom boundaries (Figure 1b). The threshold invading pressure for each site on the fracture plane is calculated according to aperture and interface geometries. The site which is connected to the invasion boundary (nonwetting fluid) and has the smallest threshold invading pressure is identified and invaded. This event modifies the list of available sites connected to the nonwetting phase, and again, available sites are sorted and the site with the smallest pressure is invaded, and so on. We take into account defending phase trapping; that is, the sites that are surrounded by the invading fluid are removed from the list of available sites.

The threshold invading pressure, assuming that the pressure in the defending phase is negligible, is calculated according to the Young-Laplace equation as

$$P_c = 2\gamma H = \gamma(k_1 + k_2) = \gamma\left(\frac{1}{r_1} + \frac{1}{r_2}\right), \tag{2}$$

where γ is the interfacial tension (here taken to be $\gamma = 72$ mN/m, considering an air-water system at a temperature of 25 °C), H is the mean curvature, $k_1 = 1/r_1$ and $k_2 = 1/r_2$ are the two principal curvatures with radii r_1 and r_2, respectively. k_1 is termed the out-of-plane or aperture-induced curvature, and k_2 is the in-plane curvature. Assuming that the fracture walls are symmetric about a mean plane, r_1 is related to the local aperture b and the contact angle θ as $r_1 = b/(2\cos\theta)$. The aperture-induced radius r_1 is always positive since b is always positive and for strong drainage we have $0 \leq \theta \ll 90°$. To compute the in-plane curvature k_2, we use the adaptive circle-fitting method proposed by Yang et al. (2012). In this method, the in-plane radius of curvature r_2 is adaptively computed by fitting a circle using the coordinates of the neighboring interfaces sites to a local point (Figure S1 in the supporting information [SI]). Note that, in contrast to r_1, the radius of curvature r_2 can be either positive or negative, depending on whether the fluid-fluid interface is convex or concave, respectively (Figure S1 in the SI).

When the fracture aperture is very small, the in-plane curvature k_2 can be neglected by assuming it to be much smaller than k_1 (or r_1 much smaller than r_2). If this assumption is valid, then the invading pressure can be approximated as $P_{\text{inv}} \approx 2\gamma\cos\theta/b$. This assumption has been invoked in modeling multiphase flow through rough fractures (Wagner et al., 1997, 1999; Ye et al., 2015, 2017). Here we investigate also the extent to which neglecting the in-plane curvature is a valid assumption.

3. Impact of Aperture Heterogeneity on Capillary Pressure Behavior

3.1. Capillary Pressure Behavior in a Random Fracture

It is useful to first consider the behavior of P_c for a spatially uncorrelated random aperture field, in the absence of confining stress. This case is an end-member case for later comparison with aperture fields generated from self-affine fracture surfaces. We generate 60 random uniformly distributed fracture aperture fields with mean $b = 1.5$ mm and coefficient of variation $\delta = 0.57$. Here, the fracture dimension is the same as the one described previously (0.65 m × 0.65 m).

We run simulations of capillary invasion using the standard IP and the MIP models and track the *local* capillary pressure, P_c, by reporting for each invaded location the threshold pressure required for an invasion to occur. The threshold capillary pressure for a given pixel changes as the invasion front advances and is updated according to equation (2). We apply a spatial medium filter with a distance of 2 pixels (on each side of the invaded location) to remove numerical artifacts brought by the jagged numerical interface. Our record of P_c is a measure of the *minimum* capillary pressure required for an invasion to occur at each menisci configuration. Similar measurements in porous media have been obtained experimentally (Aker et al., 2000; Biswas et al., 2018; Moebius & Or, 2014; Moura et al., 2017). These experiments were conducted at very low flow rates, where it was assumed that the measured capillary pressure is the local capillary pressure. Recent numerical simulations in porous media have also used the local capillary pressure from the IP invasion to investigate pressure and saturation relations for different sample sizes (Moura et al., 2015).

As an example, we show, in Figure 2a, P_c records from IP simulations with and without in-plane curvature for a completely uncorrelated uniformly distributed fracture aperture field. As expected, P_c values in both

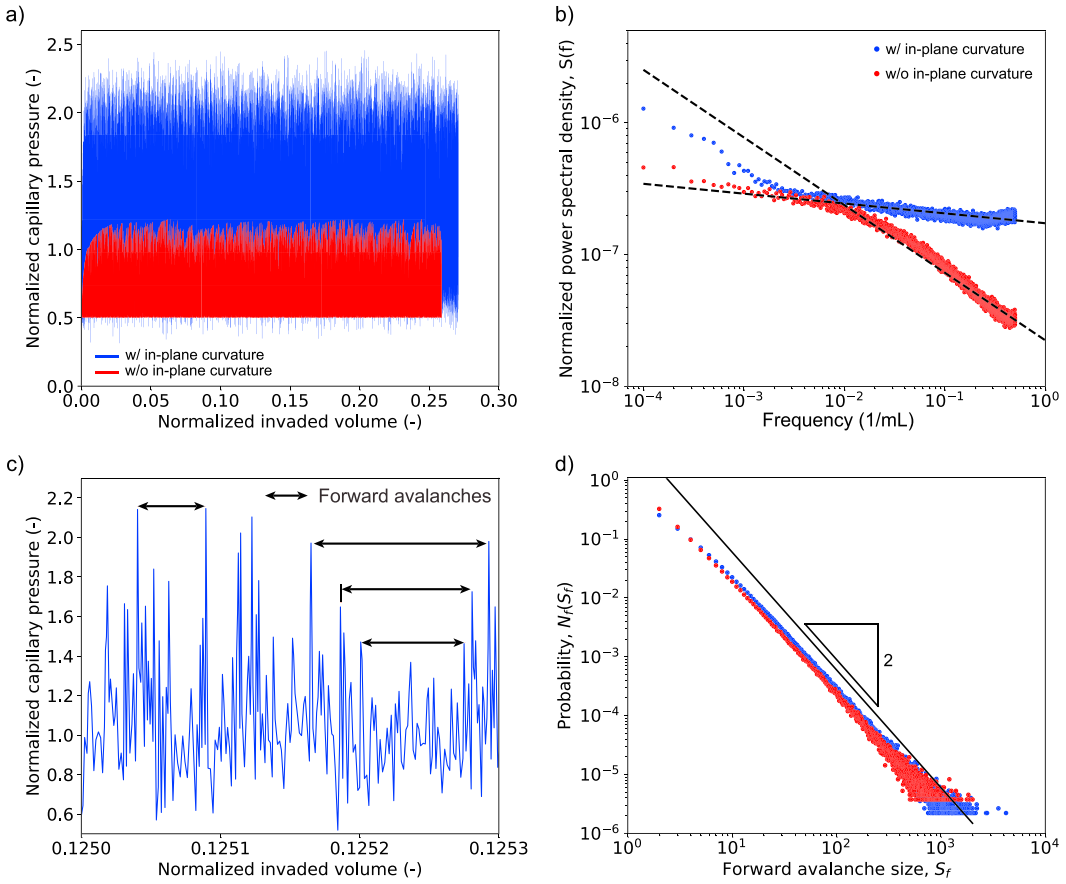

Figure 2. Behavior of capillary pressure (P_c) during invasion percolation (IP) invasion in a uniform-distributed random fracture aperture field. (a) P_c variation for IP with (blue) and without (red) in-plane curvature. P_c is normalized by the capillary pressure computed using the average fracture aperture. (b) Average power spectral density of the normalized P_c for IP with and without in-plane curvature. The black dashed lines are linear fits to the data and have slopes $\beta \approx 0.07$ and $\beta \approx 0.51$ for IP models with and without in-plane curvature, respectively. (c) Definition of hierarchical avalanches according to Maslov (1995) and Furuberg et al. (1996). (d) Distribution of hierarchical avalanche sizes for a random fracture for IP with and without in-plane curvature. Both follow a power law distribution with exponent $\alpha = 2$, in agreement with the theoretical exponent for self-organized criticality (Maslov, 1995).

cases appear uncorrelated and without any macroscopic structure. The minimum value of the normalized P_c without in-plane curvature is not a constant of 0.5 but instead shows variations that can be observed when a narrow range of invaded volumes is shown. Invasion percolation with in-plane curvature results in larger P_c. This result of larger P_c is consistent with displacement processes where the invading fluid flows through small aperture areas inaccessible to invasion in the case of IP without in-plane curvature, thus reducing the amount of trapping of the defending fluid (Yang et al., 2016).

The power spectral density, $S(f)$, of the capillary pressure record reveals the connection between P_c and the structure of the aperture field. It also elucidates the impact of considering the in-plane curvature in our IP simulations. To compute $S(f)$, we use the Welch method (Welch, 1967). Our results suggest that $S(f)$ follows a power law $S(f) \propto f^{-\beta}$, with $\beta \approx 0.38$ and $\beta \approx 0.51$ for IP model with and without in-plane curvature, respectively (Figure 2b). Thus, despite our random uncorrelated fracture aperture structure, the invasion process self-organizes, although weakly, resulting in nonflat $S(f)$.

To further validate the P_c records from our numerical simulations, we use well-established scaling laws for the occurrence of hierarchical forward avalanches, $N_f(S_f)$, which have been employed to characterize drainage in porous media (Aker et al., 2000; Biswas et al., 2018; Furuberg et al., 1996; Maslov, 1995) (Figures 2c and 2d). The scaling behavior of $N_f(S_f)$ is valid for a broad class of models that are known to self-organize in critical states (self-organized criticality model), such as IP in porous media (Maslov, 1995; Paczuski et al., 1996), landslide and forest fire occurrence (Turcotte et al., 2002), and earthquake

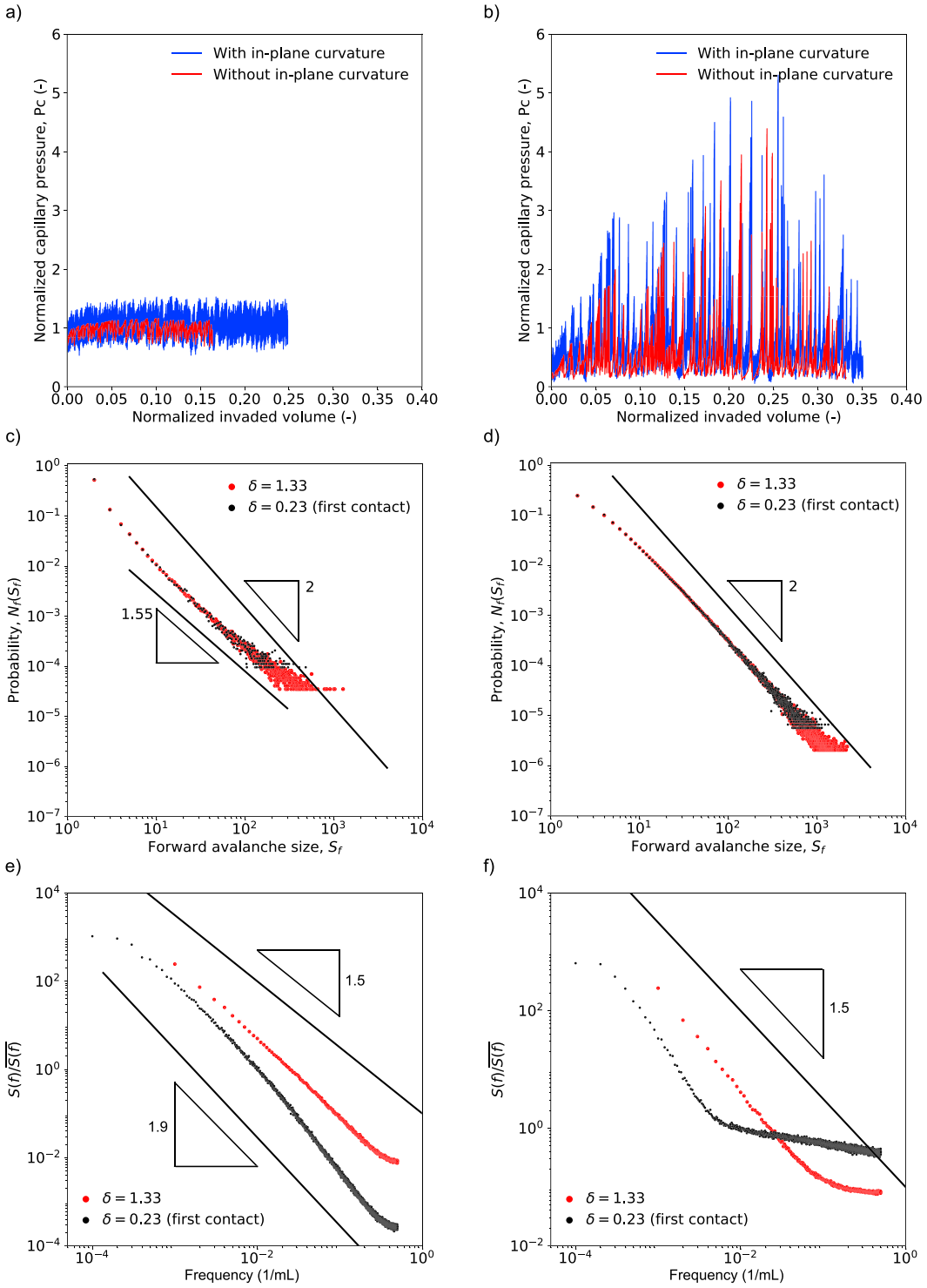

Figure 3. Behavior of capillary pressure (P_c) for invasion percolation (IP) models with and without in-plane curvature and for self-affine fracture surfaces at two different confining stresses. In these two cases, the mismatch length scale is fixed at $L_c = L/8$. (a) P_c for IP with and without in-plane curvature for fracture aperture fields containing one location of contact ($\delta = 0.23$, first contact). (b) Same as (a) but for a confining stress of $\sigma_n = 0.4$ MPa ($\delta = 1.33$). In both cases P_c is normalized by the capillary pressure computed using the respective average fracture aperture. (c) Distribution of avalanche sizes, $N_f(S_f)$, for IP *without* in-plane curvature and different confining stresses. (d) Same as (c) but for IP *with* in-plane curvature. (e) Power spectral density, $S(f)$, of P_c for IP without in-plane curvature and different confining stresses. (f) Same as (e) but for IP with in-plane curvature.

frequency-magnitude scaling (Bak & Tang, 1989). In the context of drainage in porous and fractured media, the distribution of avalanches informs whether the invasion occurs via events of relatively homogeneous sizes (narrow avalanche size distribution) or, instead, via events of very disparate sizes (e.g., a wide power law distribution for which one cannot define a standard deviation).

Thus, similar to the drainage processes in porous media, the rapid capillary pressure fluctuations observed in our numerical simulations are associated with avalanches or bursts of activity (Måløy et al., 1992). An avalanche starts when P_c drops suddenly and stops when P_c increases to a value above the pressure that initiated the burst (Figure 2c). Therefore, an avalanche may consist of a large pressure valley containing a hierarchical distribution of smaller pressure jumps within it (Figure 2c). Avalanches are associated with fluid advancement through areas of larger fracture apertures, associated with low capillary entry pressure values, up to the point where its advancement stops at an area of small fracture aperture, which requires the capillary pressure to increase in order to overcome the new barrier.

For a broad class of models with intermittent behavior, under the condition that the measured capillary pressure is the local capillary pressure, Maslov (1995) showed that the probability distribution of forward avalanches, $N_f(S_f)$, follows a power law

$$N_f(S_f) = S_f^{-\alpha}, \tag{3}$$

where S_f is the forward avalanche size, defined as the number of invaded sites during an avalanche. The power law exponent α was predicted to be $\alpha = 2$ for all invasion models showing intermittent behavior of activity (Maslov, 1995). For our completely random fracture aperture, our measurements of the distribution of avalanche sizes, using both IP models, are in good agreement with the theoretical exponent predicted by Maslov (1995; Figure 2d). Our results are also consistent with previous numerical simulations performed by Furuberg et al. (1996), who obtained $\alpha = 2.00 \pm 0.01$ for a porous media case, experiments performed by (Aker et al., 2000), using a porous media composed of glass beads, where $\alpha = 1.9 \pm 0.1$, and drying experiments reported by Biswas et al. (2018), where $\alpha = 1.99 \pm 0.05$. This agreement points to the validity of the P_c records from our simulations of quasi-static drainage in rough fractures, which we analyze further next.

3.2. Capillary Pressure Behavior in a Self-Affine Fracture

We now explore the behavior of the local capillary pressure, P_c, during slow drainage through fracture aperture fields generated from self-affine fracture surfaces.

For fracture surfaces at first contact (no confining stress), P_c for IP with and without in-plane curvature show similar mean variations that are proportional to the mean fracture aperture (Figure 3a). As expected, IP without in-plane curvature does not invade small aperture areas, resulting in smaller invading phase saturation (Yang et al., 2012). For highly stressed fracture surfaces, the standard and modified IP models show large drops in P_c that occur when the invading fluid reaches an area of large fracture aperture, as revealed by the records of local P_c fluctuations during invasion (Figure 3b). The capillary pressure then increases gradually as the invading fluid moves into the small fracture aperture areas. The invading fluid then breaks into another area of large fracture aperture and the process repeats. This process is more evident for very heterogeneous fracture apertures, as is the case for high confining stress (Figure 3b). In this case, the large P_c variations are related to the increase in fracture surface contact area and the reduction of the mean aperture when a confining stress is applied (Figure 1b).

The *local* coefficient of variation ($\delta = \sigma_b/\bar{b}$), which quantifies the degree of variability of the aperture field relative to the mean aperture, controls whether IP with and without in-plane curvature, and for fracture aperture at any confining stress amount, will yield similar results. The coefficient of variation controls the roughening and smoothing of the fluid-fluid interface and consequently the degree to which the in-plane curvature can impact P_c. For a self-affine fracture surface with nearly constant σ_b throughout the domain, locally large δ values will result from locally small aperture values, a situation that leads to small differences between the two IP models. Smaller δ values, on the contrary, correspond to larger mean aperture values, where the in-plane curvature has larger impact on P_c, resulting in larger differences between the two IP models.

We quantify the avalanche behavior during invasion, using the standard and modified IP models, by computing the probability distribution of forward avalanche sizes, $N_f(S_f)$ (equation (3)). We find that, for the standard IP model where in-plane curvature is neglected, the probability of forward avalanches follows a

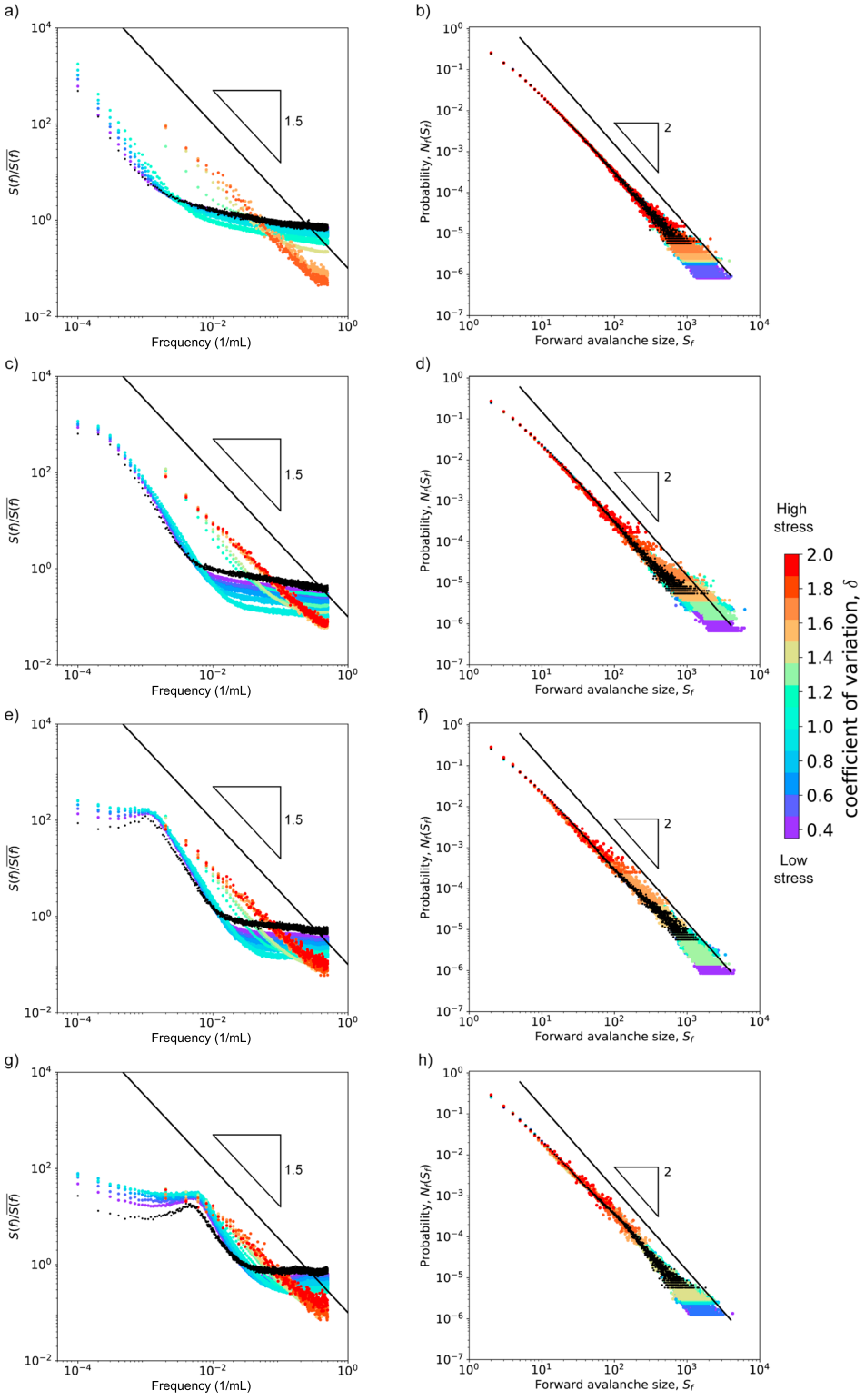

Figure 4. Capillary pressure power spectrum $S(f)$ (left column) and avalanche size distribution $N_f(S_f)$ (right column) as a function of confining stress and fracture aperture correlation length scale for invasion percolation model *with* in-plane curvature. (a, c, e, g) $S(f)$ for $L_c = L/8$, $L/16$, $L/32$, and $L/64$, respectively. (b, d, f, h) $N_f(S_f)$ for $L_c = L/8$, $L/16$, $L/32$, and $L/64$, respectively. The black dots represent results for fracture surfaces at first contact. The solid line with slope −1.5, for $S(f)$, is a guide-to-eye line to indicate the approximate slope for results at high confining stresses (larger δ values). The solid lines with slope −2, for $N_f(S_f)$ distribution, represent the theoretical power law decay for avalanche size distribution from Maslov (1995).

power law $N_f(S_f) \propto S_f^{-\alpha}$, with $\alpha \approx 1.55$ (Figure 3c). In contrast, for the modified IP model where in-plane curvature is accounted for, the same avalanche size distribution also follows a power law but with $\alpha \approx 2$ (Figure 3d). In both cases, the power law exponent α does not change as the fracture aperture changes from first contact case to the highly stressed case. Our expectation for $\alpha = 2$ exponent is due to (1) the theoretical results for SOC processes (Maslov, 1995), (2) the fact that a similar exponent is observed for porous media displacements (Aker et al., 2000; Biswas et al., 2018; Furuberg et al., 1996), and most importantly (3) the fact that this is the exponent observed for purely random fractures with no spatial correlation in the fracture gap (Figure 2). The fact that the distribution of avalanche sizes for IP without in-plane curvature deviates from the theoretical power law with exponent $\alpha = 2$ (Figure 3c) suggests that it lacks the necessary physics to properly model the invasion process through a self-affine rough fracture. Therefore, our results support the validity of the MIP model with in-plane curvature as the rough fracture analogue of the IP model in porous media, even for very highly stressed fracture surfaces.

To further quantify the differences between the capillary pressure behavior during invasion for IP models with and without in-plane curvature, we computed the power spectral density, $S(f)$, of P_c. For IP model without in-plane curvature, $S(f)$ decays as a power law for nearly all frequencies (Figure 3e). IP with in-plane curvature, in contrast, exhibits a decay in $S(f)$ at low frequencies but a stagnation at high frequencies (Figure 3f). Thus, our results indicate a decrease of self-organization when in-plane curvature is included. This decrease in self-organization appears to be larger for fracture surfaces at first contact, in agreement with the notion that in-plane curvature dominates the P_c behavior for very large fracture apertures ($1/r_2 \gg 1/r_1$ in equation (3)).

Finally, for a self-affine surface at first contact, we have verified that the scaling exponent for the distribution of avalanche sizes, α, and the behavior of $S(f)$ of P_c are almost insensitive to the grid size (see Figures S2 and S3 in the SI). Thus, in the remainder of the paper, we use a grid of $1,024 \times 1,024$ pixels.

3.3. Impact of Confining Stress on Capillary Pressure Behavior

We focus on a self-affine fracture, with different correlation lengths, and we now investigate the impact of confining stress on the capillary pressure behavior. Here, we concentrate on results with the MIP model where in-plane curvature is used, since this model incorporates the necessary physics to reproduce the expected scaling of forward avalanches. The results shown in this section were produced by averaging, for each stress level, the results of 20 statistically similar fracture apertures generated using different random number seeds.

At high confining stresses, $S(f)$ follows a power law as $S(f) \propto f^{-\beta}$, with $\beta \approx 1.5$, for the entire frequency range and for all fracture correlation length scales, L_c (Figures 4a, 4c, 4e, and 4g). As the confining stress decreases, and for all L_c cases shown here, $S(f)$ tends to nearly white noise at high frequencies. At low frequencies, $S(f)$ tends to flatten as the fracture aperture correlation length scale decreases from $L_c = L/8$ to $L_c = L/64$. Thus, our numerical simulations indicate a decrease in self-organization of the invasion process as the confining stress decreases and when fracture aperture correlation becomes smaller. It is interesting that the impact of these sources of fracture aperture heterogeneity in the $S(f)$ of P_c is in separate ranges of the power spectrum: a decrease in stress flattens the high frequencies, whereas a decrease in correlation length flattens the low frequencies.

Finally, we have verified that the distribution of avalanche sizes decays as a power law $N(s) \propto s^{-\alpha}$, with the exponent $\alpha = 2$ being independent of the applied confining stress and the fracture correlation length (Figures 4b, 4d, 4f, and 4h). This result points to the validity of the P_c measurements reported in our numerical simulations for different confining stresses, and for different aperture correlation lengths, using the MIP model that accounts for fluid-fluid curvature. In contrast, the distribution of avalanche sizes for IP without in-plane curvature does not follow a power law decay with $\alpha = 2$, suggesting that the theoretical universal scaling is only recovered in the modified IP model (Figure S4 of the SI).

4. Discussion and Conclusions

Moura et al. (2017) observed a transition in the power spectrum of P_c during drainage in porous media, from $1/f$ at low frequencies to $1/f^2$ at higher frequencies, which they could explain due to the exponential viscous relaxation following a burst in their experimental system. As our system is strictly quasi-static with no viscous dissipation, we suspect that the origin of self-organization in our model is intimately related to

the coefficient of variation of the fracture aperture, $\delta = \sigma_b/\bar{b}$, and that the transition we observe is related to *spatial* organization, rather than to *temporal* organization. For $\delta < 1$ (low stress), the in-plane curvature dominates the aperture-induced curvature ($1/r_1 \ll 1/r_2$ in equation (2)), since the average fracture aperture is larger than the aperture standard deviation. For $\delta > 1$, the opposite occurs ($1/r_2 \ll 1/r_1$), since the average fracture aperture is smaller than the aperture standard deviation, and thus, the in-plane curvature has a smaller impact on P_c. We hypothesize that the departure from self-organization at high frequencies can be attributed to the preponderance of *negative* in-plane curvatures at high stress, where the low-aperture regions act as "pinning sites" for the evolution of the interface (Jung et al., 2016; Primkulov et al., 2018).

The observation that our recorded distribution of forward avalanche sizes, $N_f(S_f)$, decays as a power law, $N_f(S_f) \propto S_f^{-2}$, is new for the MIP model in rough fractures. This broad property of the MIP model suggests that it may embody the key physics for simulating slow immiscible displacement through rough fractures, in contrast with the original IP model. Since the MIP model is quasi-static, however, it does not permit investigating the cumulative distribution of Haines jumps (Haines, 1930), a phenomenon that has been extensively studied, accompanied by avalanches, in similar investigations in porous media (Berg et al., 2013; Furuberg et al., 1996; Måløy et al., 1992; Moebius & Or, 2014; Moura et al., 2015, 2017).

We have shown that a key parameter controlling the behavior of P_c in a rough fracture is the coefficient of variation $\delta = \sigma_b/\bar{b}$. For a self-affine fracture, we observe the evolution of P_c from a weakly self-organized state at low δ values, at low confining stress and for fracture surfaces with large correlation length, to a strongly self-organized state at large δ values, at high confining stress and fracture surfaces with small correlation length. Here, we have employed a global δ value and assumed that it is representative of the entire fracture. It is likely that local δ variations are also relevant, because in the evaluation of P_c only a few sites near the would-be-invaded location are used in the computation of the in-plane curvature, suggesting that P_c may be sensitive to δ changes throughout the fracture domain, as, for example, in the case of correlated fracture surfaces (Yang et al., 2016). Further numerical investigation is required to fully understand the impact of heterogeneous δ on the behavior of P_c.

While the impact of in-plane curvature on slow drainage in rough fractures was not considered in several earlier studies (e.g., Amundsen et al., 1999; Murphy & Thomson, 1993; Wagner et al., 1997, 1999; Ye et al., 2015, 2017), our comparison between IP with and without in-plane curvature shows that the original IP model deviates from the theoretical scaling of hierarchical avalanche sizes, supporting the notion that in-plane curvature is an important mechanism in modeling immiscible flow displacement, even at large confining stresses and large degrees of fracture aperture correlation.

Correlated fracture aperture fields and variations in the normal confining stress are distinct mechanisms that can result in different degrees of fracture aperture heterogeneity. Interestingly, our results indicate that each mechanism impacts the capillary pressure during slow drainage in a different range of the P_c power spectrum. In both cases, we show that the slow drainage behavior becomes less self-organized when both the fracture aperture correlation length and the confining stress decrease. These observations, which are absent from the avalanche size distribution, point to the additional information encoded in the P_c power spectrum. In particular, our results show that an increase in confining stress is responsible for a shift of the cutoff frequency for self-organized behavior to higher frequencies (Figures 4a, 4c, 4e, and 4g). This transition frequency has been ascribed to physical properties of porous media (Moura et al., 2017) and could also be indicative of flow properties of a rough fracture (e.g., permeability-to-porosity ratio). In solving the contact problem, we have not accounted for shear stress along the fracture surfaces, the presence of gouge in the fracture aperture, and additionally, we assumed elastic deformation of the fracture surfaces. Despite these simplifications, our model indicates that the degree of heterogeneity in the fracture aperture field can be characterized using the power spectrum of P_c.

Measurements of P_c during slow drainage through porous media are reported routinely (Biswas et al., 2018; Furuberg et al., 1996; Måløy et al., 1992; Moebius & Or, 2014; Moura et al., 2015, 2017; Ramstad & Hansen, 2006). However, to the best of our knowledge, P_c measurements during slow drainage through a rough fracture, for a flow rate controlled boundary condition, have only been reported in the pioneer experimental work of Persoff and Pruess (1995). Although we recognize that measuring P_c variations at very slow flow rates can be challenging due to low signal-to-noise ratio, we hope that our numerical results will raise scientific interest to investigate experimentally P_c variations during drainage through rough fractures.

Acknowledgments
This work was funded in part by the U.S. Department of Energy (Grant DE-SC0018357 to R. J.). P. K. K. acknowledges a grant from Korea Environment Industry and Technology Institute (KEITI) through Subsurface Environmental Management (SEM) Project, funded by the Korea Ministry of Environment (MOE) (2018002440003). Z. Y. acknowledges financial support from the National Natural Science Foundation of China (41877203). No data were used in producing this manuscript.

References

Aker, E., Måløy, K. J., Hansen, A., & Basak, S. (2000). Burst dynamics during drainage displacements in porous media: Simulations and experiments. *Europhysics Letters*, *51*(1), 55–61. https://doi.org/10.1209/epl/i2000-00331-2

Amundsen, H., Wagner, G., Oxaal, U., Meakin, P., Feder, J., & Jøssang, T. (1999). Slow two-phase flow in artificial fractures: Experiments and simulations. *Water Resources Research*, *35*(9), 2619–2626. https://doi.org/10.1029/1999WR900147

Andrews, D. (1988). On modeling closure of rough surfaces in contact. *Eos, Transactions of the American Geophysical Union*, *69*, 1426–1427.

Auradou, H., Måløy, K. J., Schmittbuhl, J., & Hansen, A. (2003). Drainage in a rough gouge-filled fracture. *Transport in Porous Media*, *50*(3), 267–305. https://doi.org/10.1023/A:1021164109061

Bak, P., & Tang, C. (1989). Earthquakes as a self-organized critical phenomenon. *Journal of Geophysical Research*, *94*(B11), 15,635–15,637. https://doi.org/10.1029/JB094iB11p15635

Berg, S., Ott, H., Klapp, S. A., Schwing, A., Neiteler, R., Brussee, N., et al. (2013). Real-time 3D imaging of Haines jumps in porous media flow. *Proceedings of the National Academy of Sciences*, *110*(10), 3755–3759. https://doi.org/10.1073/pnas.1221373110

Bertels, S. P., DiCarlo, D. A., & Blunt, M. J. (2001). Measurement of aperture distribution, capillary pressure, relative permeability, and in situ saturation in a rock fracture using computed tomography scanning. *Water Resources Research*, *37*(3), 649–662. https://doi.org/10.1029/2000WR900316

Biswas, S., Fantinel, P., Borgman, O., Holtzman, R., & Goehring, L. (2018). Drying and percolation in correlated porous media. *Physical Review Fluids*, *3*(12), 124–307. https://doi.org/10.1103/PhysRevFluids.3.124307

Broadbent, S., & Hammersley, J. (1957). Percolation processes. I. Crystals and mazes. *Proceedings of the Cambridge Philosophical Society*, *53*(3), 629–641.

Brooks, R. H., & Corey, A. T. (1964). Hydraulic properties of porous media. *Hydrology Papers*, *3*(3), 27.

Brown, S. (1995). Simple mathematical model of a rough fracture. *Journal of Geophysical Research*, *100*(B4), 5941–5952. https://doi.org/10.1029/94JB03262

Brown, S., & Scholz, C. (1985a). Broad bandwidth study of the topography of natural rock surfaces. *Journal of Geophysical Research*, *90*(B14), 2575–2582. https://doi.org/10.1029/JB090iB14p12575

Brown, S., & Scholz, C. (1985b). Closure of random elastic surfaces in contact. *Journal of Geophysical Research*, *90*(NB7), 5531–5545. https://doi.org/10.1029/JB090iB07p05531

Chen, Y.-F., Fang, S., Wu, D.-S., & Hu, R. (2017). Visualizing and quantifying the crossover from capillary fingering to viscous fingering in a rough fracture. *Water Resources Research*, *53*, 7756–7772. https://doi.org/10.1002/2017WR021051

Chen, Y.-F., Guo, N., Wu, D.-S., & Hu, R. (2018). Numerical investigation on immiscible displacement in 3D rough fracture: Comparison with experiments and the role of viscous and capillary forces. *Advances in Water Resources*, *118*, 39–48. https://doi.org/10.1016/j.advwatres.2018.05.016

Chen, Y.-F., Wu, D.-S., Fang, S., & Hu, R. (2018). Experimental study on two-phase flow in rough fracture: Phase diagram and localized flow channel. *International Journal of Heat and Mass Transfer*, *122*, 1298–1307. https://doi.org/10.1016/j.ijheatmasstransfer.2018.02.031

Furuberg, L., Måløy, K. J., & Feder, J. (1996). Intermittent behavior in slow drainage. *Physical Review E*, *53*(1), 966–977. https://doi.org/10.1103/PhysRevE.53.966

Glass, R. J., Nicholl, M. J., & Yarrington, L. (1998). A modified invasion percolation model for low-capillary number immiscible displacements in horizontal rough-walled fractures: Influence of local in-plane curvature. *Water Resources Research*, *34*(12), 3215–3234. https://doi.org/10.1029/98WR02224

Glass, R. J., Rajaram, H., & Detwiler, R. L. (2003). Immiscible displacements in rough-walled fractures: Competition between roughening by random aperture variations and smoothing by in-plane curvature. *Physical Review E*, *68*(6), 61110. https://doi.org/10.1103/PhysRevE.68.061110

Haines, W. B. (1930). Studies in the physical properties of soil. V. The hysteresis effect in capillary properties, and the modes of moisture distribution associated therewith. *The Journal of Agricultural Science*, *20*(01), 97–116. https://doi.org/10.1017/S002185960008864X

Holtzman, R., Szulczewski, M. L., & Juanes, R. (2012). Capillary fracturing in granular media. *Physical Review Letters*, *108*(26), 264–504. https://doi.org/10.1103/PhysRevLett.108.264504

Huo, D., & Benson, S. M. (2016). Experimental investigation of stress-dependency of relative permeability in rock fractures. *Transport in Porous Media*, *113*(3), 567–590. https://doi.org/10.1007/s11242-016-0713-z

Jaeger, J. C., & Cook, N. G. W. (1979). *Fundamentals of rock mechanics*. London: Chapman and Hall.

Jung, M., Brinkmann, M., Seemann, R., Hiller, T., Sanchez de La Lama, M., & Herminghaus, S. (2016). Wettability controls slow immiscible displacement through local interfacial instabilities. *Physical Review Fluids*, *1*(7), 74,202. https://doi.org/10.1103/PhysRevFluids.1.074202

Kang, P. K., Brown, S., & Juanes, R. (2016). Emergence of anomalous transport in stressed rough fractures. *Earth and Planetary Science Letters*, *454*, 46–54.

Lenormand, R., Touboul, E., & Zarcone, C. (1988). Numerical models and experiments on immiscible displacements in porous media. *Journal of Fluid Mechanics*, *189*, 165–187. https://doi.org/10.1017/S0022112088000953

Lenormand, R., Zarcone, C., & Sarr, A. (1983). Mechanisms of the displacement of one fluid by another in a network of capillary ducts. *Journal of Fluid Mechanics*, *135*(-1), 337–353. https://doi.org/10.1017/S0022112083003110

Lian, P., & Cheng, L. (2012). The characteristics of relative permeability curves in naturally fractured carbonate reservoirs. *Journal of Canadian Petroleum Technology*, *51*(02), 137–142. https://doi.org/10.2118/154814-PA

Måløy, K., Furuberg, L., Feder, J., & Jøssang, T. (1992). Dynamics of slow drainage in porous media. *Physical Review Letters*, *68*(14), 2161–2164. https://doi.org/10.1103/PhysRevLett.68.2161

Maslov, S. (1995). Time directed avalanches in invasion models. *Physical Review Letters*, *74*(4), 562. https://doi.org/10.1103/PhysRevLett.74.562

Mavko, G., Mukerji, T., & Dvorkin, J. (2009). *The rock physics handbook: Tools for seismic analysis of porous media* (2nd ed.). Cambridge,K: Cambridge University Press.

McDonald, A., Beckner, B., Chan, H., Jones, T., & Wooten, S. (1991). *Some important considerations in the simulation of naturally fractured reservoirs*. Dallas, TX: Society of Petroleum Engineers. https://doi.org/10.2118/21814-MS

Meakin, P., Feder, J., Frette, V., & T. Jøssang (1992). Invasion percolation in a destabilizing gradient. *Physical Review A*, *46*(6), 3357–3368. https://doi.org/10.1103/PhysRevA.46.3357

Moebius, F., & Or, D. (2014). Pore scale dynamics underlying the motion of drainage fronts in porous media. *Water Resources Research*, *50*, 8441–8457. https://doi.org/10.1002/2014WR015916

Moura, M., Fiorentino, E.-A., Måløy, K. J., Schäfer, G., & Toussaint, R. (2015). Impact of sample geometry on the measurement of pressure-saturation curves: Experiments, and simulations. *Water Resources Research*, *51*, 8900–8926. https://doi.org/10.1002/2015WR017196

Moura, M., Måløy, K. J., & Toussaint, R. (2017). Critical behavior in porous media flow. *EPL*, *118*(1), 14,004. https://doi.org/10.1209/0295-5075/118/14004

Murphy, J. R., & Thomson, N. R. (1993). Two-phase flow in a variable aperture fracture. *Water Resources Research*, *29*(10), 3453–3476. https://doi.org/10.1029/93WR01285

Neuweiler, I., Sorensen, I., & Kinzelbach, W. (2004). Experimental and theoretical investigations of drainage in horizontal rough-walled fractures with different correlation structures. *Advances in Water Resources*, *27*(12), 1217–1231. https://doi.org/10.1016/j.advwatres.2004.07.005

Nuske, P., Faigle, B., Helmig, R., Niessner, J., & Neuweiler, I. (2010). Modeling gas-water processes in fractures with fracture flow properties obtained through upscaling. *Water Resources Research*, *46*, W09528. https://doi.org/10.1029/2009WR008076

Paczuski, M., Maslov, S., & Bak, P. (1996). Avalanche dynamics in evolution, growth, and depinning models. *Physical Review E*, *53*(1), 414–443. https://doi.org/10.1103/PhysRevE.53.414

Persoff, P., & Pruess, K. (1995). Two-phase flow visualization and relative permeability measurement in natural rough-walled rock fractures. *Water Resources Research*, *31*(5), 1175–1186. https://doi.org/10.1029/95WR00171

Power, W., & Tullis, T. (1991). Euclidean and fractal models for the description of rock surface-roughness. *Journal of Geophysical Research*, *96*(B1), 415–424. https://doi.org/10.1029/90JB02107

Primkulov, B. K., Talman, S., Khaleghi, K., Rangriz Shokri, A., Chalaturnyk, R., Zhao, B., et al. (2018). Quasistatic fluid-fluid displacement in porous media: Invasion-percolation through a wetting transition. *Physical Review Fluids*, *3*(10), 104001. https://doi.org/10.1103/PhysRevFluids.3.104001

Pruess, K. (2008). Leakage of CO_2 from geologic storage: Role of secondary accumulation at shallow depth. *International Journal of Greenhouse Gas Control*, *2*(1), 37–46. https://doi.org/10.1016/S1750-5836(07)00095-3

Pyrak-Nolte, L. J., Cook, N., & Myer, L. (1990). A stratified percolation model for saturated and unsaturated flow through natural fractures. Amer Nuclear Soc.

Pyrak-Nolte, L. J., & Morris, J. P. (2000). Single fractures under normal stress: The relation between fracture specific stiffness and fluid flow. *International Journal of Rock Mechanics and Mining Sciences*, *37*(1-2), 245–262. https://doi.org/10.1016/S1365-1609(99)00104-5

Pyrak-Nolte, L. J., & Nolte, D. D. (2016). Approaching a universal scaling relationship between fracture stiffness and fluid flow. *Natural Computing*, *7*(10), 663. https://doi.org/10.1038/ncomms10663

Ramstad, T., & Hansen, A. (2006). Cluster evolution in steady-state two-phase flow in porous media. *Physical Review E*, *73*(2), 26,306. https://doi.org/10.1103/PhysRevE.73.026306

Reitsma, S., & Kueper, B. H. (1994). Laboratory measurement of capillary pressure-saturation relationships in a rock fracture. *Water Resources Research*, *30*(4), 865–878. https://doi.org/10.1029/93WR03451

Turcotte, D. L., Malamud, B. D., Guzzetti, F., & Reichenbach, P. (2002). Self-organization, the cascade model, and natural hazards. *Proceedings of the National Academy of Sciences*, *99*(suppl 1), 2530–2537. https://doi.org/10.1073/pnas.012582199

Unger, A. J. A., & Mase, C. W. (1993). Numerical study of the hydromechanical behavior of two rough fracture surfaces in contact. *Water Resources Research*, *29*(7), 2101–2114. https://doi.org/10.1029/93WR00516

van Genuchten, M. T. (1980). A closed-form equation for predicting the hydraulic conductivity of unsaturated soils. *Soil Science Society of America Journal*, *44*(5), 892–898. https://doi.org/10.2136/sssaj1980.03615995004400050002x

Wagner, G., Meakin, P., Feder, J., & Jøssang, T. (1997). Invasion percolation on self-affine topographies. *Physical Review E*, *55*(2), 1698–1703. https://doi.org/10.1103/PhysRevE.55.1698

Wagner, G., Meakin, P., Feder, J., & Jøssang, T. (1999). Invasion percolation in fractal fractures. *Physica A*, *264*(3–4), 321–337. https://doi.org/10.1016/S0378-4371(98)00463-4

Wang, L., & Cardenas, M. B. (2016). Development of an empirical model relating permeability and specific stiffness for rough fractures from numerical deformation experiments. *Journal of Geophysical Research: Solid Earth*, *121*, 4977–4989. https://doi.org/10.1002/2016JB013004

Watanabe, N., Sakurai, K., Ishibashi, T., Ohsaki, Y., Tamagawa, T., Yagi, M., & Tsuchiya, N. (2015). New v-type relative permeability curves for two-phase flows through subsurface fractures. *Water Resources Research*, *51*, 2807–2824. https://doi.org/0.1002/2014WR016515

Welch, P. (1967). The use of fast Fourier transform for the estimation of power spectra: A method based on time averaging over short, modified periodograms. *IEEE Transactions on Audio and Electroacoustics*, *15*(2), 70–73. https://doi.org/10.1109/TAU.1967.1161901

Wilkinson, D., & Willemsen, J. (1983). Invasion percolation: A new form of percolation theory. *Journal of Physics A (Mathematical and General)*, *16*(14), 3365–3376. https://doi.org/10.1088/0305-4470/16/14/028

Yang, Z., Neuweiler, I., Méheust, Y., Fagerlund, F., & Niemi, A. (2016). Fluid trapping during capillary displacement in fractures. *Advances in Water Resources*, *95*, 264–275. https://doi.org/10.1016/j.advwatres.2015.07.015

Yang, Z., Niemi, A., Fagerlund, F., & Illangasekare, T. (2012). A generalized approach for estimation of in-plane curvature in invasion percolation models for drainage in fractures. *Water Resources Research*, *48*, W09507. https://doi.org/10.1029/2012WR011829

Yang, Z., Niemi, A., Fagerlund, F., & Illangasekare, T. (2013). Two-phase flow in rough-walled fractures: Comparison of continuum and invasion-percolation models. *Water Resources Research*, *49*, 993–1002. https://doi.org/10.1002/wrcr.20111

Ye, Z., Liu, H.-H., Jiang, Q., Liu, Y., & Cheng, A. (2017). Two-phase flow properties in aperture-based fractures under normal deformation conditions: Analytical approach and numerical simulation. *Journal of Hydrology*, *545*, 72–87. https://doi.org/10.1016/j.jhydrol.2016.12.017

Ye, Z., Liu, H.-H., Jiang, Q., & Zhou, C. (2015). Two-phase flow properties of a horizontal fracture: The effect of aperture distribution. *Advances in Water Resources*, *76*, 43–54. https://doi.org/10.1016/j.advwatres.2014.12.001

Zimmerman, R. W., & Bodvarsson, G. S. (1996). Hydraulic conductivity of rock fractures. *Transport in Porous Media*, *23*(1), 1–30. https://doi.org/10.1007/BF00145263